


RESEARCH ARTICLE

Pacific subsurface temperature as a long-range indicator of El Niño, regional precipitation, and fire

Enoch Yan Lok Tsui^{1,2}  | Ralf Toumi^{1,3}¹Department of Physics, Imperial College London, London, UK²Leverhulme Centre for Wildfires, Environment and Society, London, UK³Grantham Institute, Imperial College London, London, UK**Correspondence**

E. Y. L. Tsui, Department of Physics, Imperial College London, London SW7 2AZ, UK.

Email: e.tsui20@imperial.ac.uk**Funding information**

Leverhulme Centre for Wildfires, Environment and Society, Grant/Award Number: RC-2018-023; Natural Environment Research Council, Grant/Award Number: NERC/UKRI NE/V017756/1; Singapore Green Finance Centre

Abstract

The SubNiño4 index based on the subsurface potential temperature around the thermocline beneath the west Pacific warm pool, the Niño 4 region, is examined as a long-range indicator of the surface El Niño–Southern Oscillation (ENSO) and ENSO-driven atmospheric response. The SubNiño4 index captures the evolution of subsurface ocean heat content between the El Niño and La Niña phases of the ENSO cycle, allowing it to serve as a long-range indicator of surface ENSO and hence also many ENSO-driven atmospheric anomalies. The SubNiño4 index has more temporally stable correlations with Niño 3.4 than the widely used western equatorial Pacific warm-water volume indicator. For a lead time of the order of 12 months, Niño 3.4 correlations afforded by the lead observed SubNiño4 index become similar to and can exceed those produced by typical dynamical ENSO predictions. The value and viability of the SubNiño4 index as a simple statistical long-range indicator of ENSO-driven atmospheric response is shown for regional precipitation anomalies throughout the Tropics and fires in Continental and Maritime Southeast Asia.

KEYWORDS

ENSO, west Pacific warm pool, west Pacific warm-water volume, subsurface temperature, tropical precipitation, Southeast Asia fire, teleconnection, Niño 3.4

1 | INTRODUCTION

El Niño (La Niña) events refer to the warming (cooling) of the equatorial Pacific Ocean sea-surface temperature (SST; Timmermann *et al.*, 2018; Wang, 2018). These conditions are accompanied by a weakening (strengthening) of the Pacific equatorial trade winds and other changes in atmospheric and oceanic circulations (Timmermann *et al.*, 2018). The Southern Oscillation refers to the oscillatory behaviour of the sea-level pressure between the tropical East and West Pacific (Wang, 2018). The warming and cooling of the equatorial Pacific SST and the Southern Oscillation are now understood as different manifestations

of the same basinwide climate phenomenon, termed El Niño–Southern Oscillation (ENSO), which is driven by coupled atmosphere–ocean processes (Timmermann *et al.*, 2018; Wang, 2018). ENSO affects global climate, marine, and terrestrial ecosystems (Timmermann *et al.*, 2018). It dominates interannual climate variability and affects seasonal precipitation, wind, and temperature patterns over vast distances globally through dynamical atmospheric processes (Davey *et al.*, 2014; Timmermann *et al.*, 2018).

Bjerknes (1969) first proposed that El Niño is brought to a mature state by a positive feedback between a warm SST anomaly and westerly wind anomaly via the SST

gradient, Walker circulation, and ocean circulation. Since then, various negative feedback mechanisms have been put forward to allow for the oscillatory behaviour of ENSO, giving rise to four different self-sustained oscillator models for ENSO: the delayed oscillator model (Suarez and Schopf, 1988; Battisti and Hirst, 1989) based on the reflection of westward-propagating downwelling Rossby waves into eastward-propagating downwelling Kelvin waves at the western boundary of the Pacific; the recharge–discharge oscillator model (Jin, 1997a; 1997b) based on the discharge and recharge of equatorial Pacific Ocean heat content to and from higher latitudes via Sverdrup transport; the western Pacific oscillator model (Weisberg and Wang, 1997; Wang *et al.*, 1999) based on the upwelling Kelvin wave forced by wind anomalies in the western Pacific; and the advective–reflective oscillator model (Picaut *et al.*, 1997) based on the anomalous zonal current associated with the reflections of upwelling Rossby (downwelling Kelvin) waves into upwelling Kelvin (downwelling Rossby) waves at the western (eastern) boundary of the Pacific and the mean zonal current. The unified oscillator model (Wang, 2001; 2018) summarises the four self-sustained oscillator models nicely, suggesting that all proposed negative feedback mechanisms are at work together, with their relative importance varying with time. It has been identified that a build-up of ocean heat content resulting from advective processes is necessary for the onset of El Niño (Ramesh and Murtugudde, 2013; Ballester *et al.*, 2016; Timmermann *et al.*, 2018). In particular, Ramesh and Murtugudde (2013) showed that a subsurface discharge of warm water always begins prior to an El Niño event and can precede the peak by up to 18 months. Thus, successful capturing of such processes holds the key to long-range ENSO forecasts (McPhaden, 2004; McGregor *et al.*, 2012; Ramesh and Murtugudde, 2013; Ballester *et al.*, 2016; Petrova *et al.*, 2017; Timmermann *et al.*, 2018).

The incorporation of subsurface temperature into statistical ENSO oceanic surface state predictions has been explored previously (e.g., Drosowsky, 2006; Petrova *et al.*, 2017; 2020). Here we extend the idea, to study directly for the first time the relationship between subsurface temperature and atmospheric responses throughout the Tropics identified to have a teleconnection with the ENSO oceanic surface state. In particular, the western Pacific warm-water volume (WWV_w) has been used as a long-range predictor for ENSO (e.g., Planton *et al.*, 2018; Izumo *et al.*, 2019; Zhao *et al.*, 2021). Here, we propose an index similar to WWV_w but based on the subsurface potential temperature (SubT) around the thermocline. The SubNiño4 index is defined to be the SubT anomaly averaged beneath the Niño 4 region between depths of 100 and 300 m. Sparks and Toumi (2020) first constructed a similar index, which they called the sub-Niño4 index, as the mean June–August “subsurface ocean

temperature anomaly” averaged over the same region, and showed that it is capable of predicting tropical cyclone landfall in South China with a lead time of one year. They attributed this success to the surfacing of the temperature anomaly around the SubNiño4 region, establishing SST patterns that influence atmospheric circulation patterns.

We show here that the SubNiño4 index captures the subsurface heat advection around halfway between the mature El Niño and La Niña phases of the ENSO cycle. The lagged correlation between the observed SubNiño4 and Niño 3.4 can exceed the simultaneous correlation between the observed and predicted ENSO at a lead time of around 12 months. We also show that the SubNiño4 index may be more reliable than the WWV_w indicator. Using regional precipitations and fires as examples, we demonstrate that the SubNiño4 index can serve as a long-range indicator of ENSO-driven atmospheric phenomena in many regions of the Tropics.

2 | DATA AND METHODS

2.1 | Datasets

Both SST and SubT data were obtained from the UK Met Office Hadley Centre observation datasets. SST data were taken from the Hadley Centre Sea Ice and Sea Surface Temperature dataset HadISST1 (Rayner *et al.*, 2003). SubT data were taken from the EN4 dataset (Good *et al.*, 2013); in particular, version EN.4.2.2 with Gouretski and Reseghetti (2010) expendable bathythermographs (XBT) and Gouretski and Cheng (2020) mechanical bathythermographs (MBT) corrections was used. Here each SubT data entry has an accompanying observation weight between 0 and 1, which is the relative weighting given to the observations compared with the background, with 0 meaning no observations.

Surface zonal wind stress data consist of the eastward turbulent surface stress taken from the European Centre for Medium-Range Weather Forecasts (ECMWF) ERA5 monthly averaged data on single levels from 1979 to the present (Hersbach *et al.*, 2019).

Two precipitation datasets were used in this study. Global precipitation data were taken from the National Oceanic and Atmospheric Administration (NOAA) National Centers for Environmental Information Global Precipitation Climatology Project (GPCP) Climate Data Record (CDR) version 2.3 (Adler *et al.*, 2016). Indian precipitation data were taken from the Indian Institute of Tropical Meteorology (IITM) Indian regional/subdivisionsal Monthly Rainfall dataset (IITM–IMR: Kothawale and Rajeevan, 2017).

Fire data were obtained from the National Aeronautics and Space Administration (NASA) Moderate Resolution

Imaging Spectroradiometer (MODIS) Collection 6 Active Fire Product (Giglio *et al.*, 2016; 2020). Fire pixels recorded in the gMCD14ML product by the *Terra* satellite were filtered to keep only those classed as “presumed vegetation fire” and with a detection confidence of at least 30%. These pixels were then adjusted for the cloud coverage recorded in the MOD14CMQ product according to Giglio *et al.* (2006). The fire count over a region is the total number of cloud-cover-adjusted pixels over that region.

The Canadian Forest Service Fire Weather Index Rating System (FWI) produced by the Copernicus Emergency Management Service for the European Forest Fire Information System (European Centre for Medium-Range Weather Forecasts, 2019) was used in this study. It gives the best dependence index skill score in Southeast Asia among the three indices studied by Di Giuseppe *et al.* (2016). The FWI depends on local noon relative humidity, temperature, and wind speed among others.

2.2 | Methods

To obtain the time series of the Niño 3.4 index, the monthly average SST data were averaged over the Niño 3.4 region (170°W–120°W, 5°S–5°N) and then the seasonal cycle computed from the 30-year period from 1986–2015 was removed. The time series of the SubNiño4 index was obtained similarly from the monthly average SubT data, averaging over the Niño 4 region (160°E–150°W, 5°S–5°N) and between depths of 100 and 300 m. Monthly average 20 °C isotherm depth (Z_{20}) profiles were determined by interpolating the monthly average SubT data vertically. The Niño4– Z_{20} anomaly time series was then obtained from the monthly average Z_{20} profiles using the same procedure as for the Niño 3.4 index, averaging over the Niño 4 region. WWV_w is the volume of water above the 20 °C isotherm within 120°E–160°W and 5°S–5°N and its anomaly time series was obtained as above. The time series of the surface zonal wind stress anomaly over the Niño 4 region was obtained similarly from the monthly average surface zonal wind stress data.

To study the behaviour of the Niño 3.4 and SubNiño4 time series, their three-month moving average time series were considered. Their mean, standard deviation, skewness, and excess kurtosis were computed. Discrete Fourier transforms were performed on the time series to obtain their frequency spectra. Peaks are considered significant if their amplitude is above the 95th percentile from an ensemble of 10,000 first-order autoregression (AR(1)) model simulations. A subsurface warm (cold) episode is defined to be the period when the SubNiño4 three-month moving average time series exceeds 0.5 °C (–0.5 °C) for at least five consecutive three-month periods.

To study the time evolution of the SubT anomaly profile, the monthly average SubT data were averaged between latitudes of 5°S and 5°N and linearly detrended. The seasonal cycle computed from the 30-year period from 1986–2015 was removed and the three-month moving average was considered. The peak of each subsurface warm and cold episode was identified and used as anchor to align all episodes. The composite difference between warm and cold episodes was taken during various three-month periods before and after the peak for up to one year and significance was determined by bootstrapping with 5,000 resamples. Correlation analysis was performed between the SubNiño4 index at the peak three-month period and the processed subsurface profile with various lead/lag for up to one year.

To investigate the connection between the surface and subsurface, the lagged correlations between the SubNiño4 index and various surface variables, including the Niño 3.4 index, precipitation, and FWI, were computed.

The Niño 3.4 index and the global precipitation field were averaged over the four main seasons of December–February (DJF), March–May (MAM), June–August (JJA), and September–November (SON). The Niño 3.4 index was correlated with the SubNiño4 index and, for benchmarking purposes, the WWV_w anomaly in the 25 overlapping three-month periods leading to each of the four main seasons. The global precipitation field was correlated with the SubNiño4 index in the three-month period exactly one year before each of the four main seasons.

Precipitation over the Maritime Continent (95°E–150°E, 12°S–5°N) DJF (King and Vincent, 2018), Northeast Brazil (47°W–35°W, 10°S–0°) MAM (Folland *et al.*, 2001), Gulf of Guinea (20°W–10°E, 4°N–8°N) and Sahel (20°W–10°E, 10°N–20°N) June–September (JJAS) (Losada *et al.*, 2012), South Africa (12.5°E–42.5°E, 35°S–15°S) December–March (DJFM) (Hoell *et al.*, 2017), and East Africa (30°E–41.25°E, 15°S–5°N) October–December (OND) (Mutai *et al.*, 1998) was correlated with the SubNiño4 index and, for benchmarking purposes, the WWV_w anomaly and Niño 3.4 index for the 25 overlapping three-month periods leading to the relevant precipitation season. The analysis was also performed on the Maritime Continent over the remaining three main seasons MAM, JJA, and SON; on East Africa MAM; and on IITM–IMR JJAS.

The analysis described above for regional precipitation was repeated for the FWI averaged over the most fire-active part of Maritime Southeast Asia (95°E–119°E, 6°S–7°N) for June–October (JASO) and Continental Southeast Asia (100°E–110°E, 9°N–17°N) DJFM. The two regions were chosen to capture most of the fire, and the peak season for the FWI over the corresponding region was chosen for study.

All time series were linearly detrended before correlation analysis. All correlation coefficients in this study are Pearson correlation coefficients.

3 | RESULTS

3.1 | Connection between sea-surface and subsurface temperatures

The Niño 3.4 and SubNiño4 time series between 1979 and 2020 are shown in Figure 1a. In general, the SubNiño4 index leads the Niño 3.4 index by a fairly constant time of about 6–12 months. The subsurface warm and cold

episodes identified are shaded in pink and cyan, respectively. Figure 1b shows the frequency spectra of the Niño 3.4 and SubNiño4 time series, together with corresponding benchmark amplitude from an AR(1) ensemble. Both frequency spectra have significant peaks corresponding to periods of 1.46 and 4.53 years. In between, Niño 3.4 shows six more significant peaks, but only two are matched by SubNiño4; just beyond the high-frequency end, Niño 3.4 displays two more significant peaks, neither of which is matched by SubNiño4. The two frequency spectra are similar overall, but SubNiño4 is less noisy. Normalised histograms of the two indices are shown in Figure 1c. The SubNiño4 index displays a higher mean, lower standard deviation, and higher kurtosis than the



FIGURE 1 (a) Time series of the SubNiño4 and Niño 3.4 indices. Subsurface warm (cold) events are indicated with pink (cyan) shading. (b) Frequency spectra of SubNiño4 and Niño 3.4. The dashed lines indicate the 95th percentile amplitude from an ensemble of 10,000 AR(1) model simulations. (c) Normalised histogram of SubNiño4 and Niño 3.4 with mean (μ), standard deviation (σ), skewness (g_1), and excess kurtosis (β_2). (d) Same as (c) but for the Niño4–Z20 anomaly. (e) Same as (c) but for the surface zonal wind stress anomaly over the Niño 4 region. (f) Observation weights for SubT at 27 different points within the SubNiño4 region (grey) and the average (pink). The red line marks the beginning of 1979 [Colour figure can be viewed at wileyonlinelibrary.com]

Niño 3.4 index. The SubNiño4 index is negatively skewed, while the Niño 3.4 index is positively skewed, with the former having a higher absolute skewness. The normalised histograms of the SubNiño4 index and the Niño4–Z20 anomaly resemble each other (Figure 1c,d). They are highly correlated ($r = 0.99$, $p < 0.01$) and have similar negative skewness. The normalised histogram of the surface zonal wind stress anomaly over the Niño 4 region is shown in Figure 1e. It is positively skewed and significantly correlated with the SubNiño4 index in December ($r = -0.34$, $p < 0.05$) and January ($r = -0.49$, $p < 0.01$). Figure 1f shows the SubT observation weights for 27 points inside the SubNiño4 region and the region-averaged observation weight from 1960–2020. To ensure data quality, only data from 1979 onwards are used in this study unless otherwise specified.

Figure 2 shows the time evolution of the composite difference of the SubT profiles between subsurface warm and cold episodes, aligned at their peaks with significance determined by bootstrapping. Figure 3 shows the correlation between the SubNiño4 index over the anchor three-month period and the SubT profiles with various lead/lag, with significance determined by p -value.

The patterns displayed in the two figures resemble each other, revealing the spatio-temporal evolution of equatorial Pacific ocean heat content during a generic ENSO cycle. The cycle begins around half a year before a subsurface warm/cold episode with a temperature anomaly centred westwards of the SubNiño4 region and connected to the surface. The temperature anomaly then extends into the SubNiño4 region to establish a subsurface warm/cold episode, while disconnecting itself from the surface. It then propagates eastwards and upwards along the climatological 20°C isotherm fully decoupled from the surface. After around half a year, the subsurface temperature anomaly starts to leave the SubNiño4 region and spreads to the surface. One year from the subsurface warm/cold episode, the temperature anomaly becomes disconnected from the isotherm and manifests itself as a purely surface temperature anomaly, replacing the temperature anomaly of opposite sign that existed there around two years ago.

Figure 4 shows the lagged correlations (r) of the SubNiño4 index and the WWV_W anomaly averaged over various three-month periods, with the Niño 3.4 index averaged over each of the four main seasons. For a broad time window one year ahead of each main season, the SubNiño4

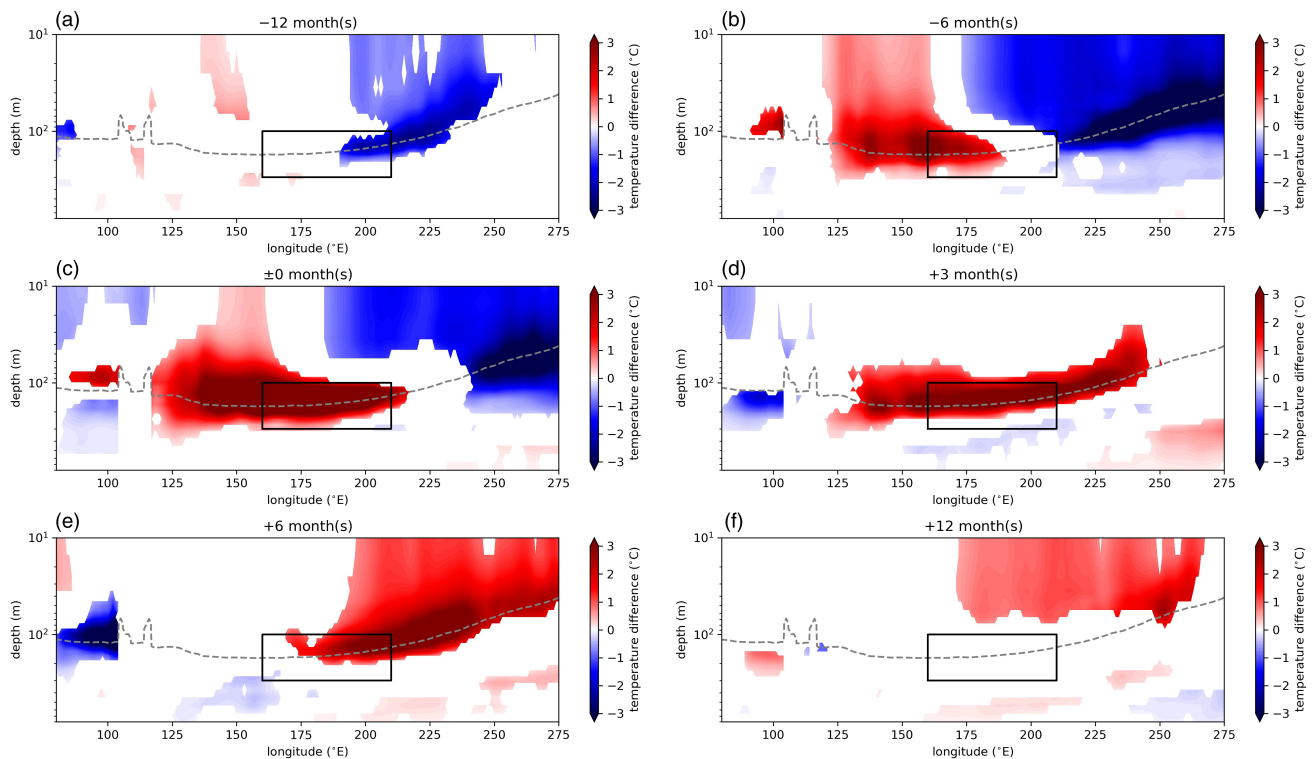


FIGURE 2 Composite difference of SubT profile averaged between 5°S and 5°N between subsurface warm and cold events with various lead/lag times. Only differences deemed significant at 95% confidence or above by bootstrapping with 5,000 resamples are shown. The dashed grey line and the black box indicate the climatological 20°C isotherm and the extent of the SubNiño4 region, respectively. Anchors for subsurface warm events: February 1981, May 1986, March 1989, October 1989, February 1997, July 2004, December 2007, August 2018; anchors for subsurface cold events: August 1983, July 1987, February 1992, May 1993, January 1995, December 1997, March 2010, January 2016 [Colour figure can be viewed at wileyonlinelibrary.com]

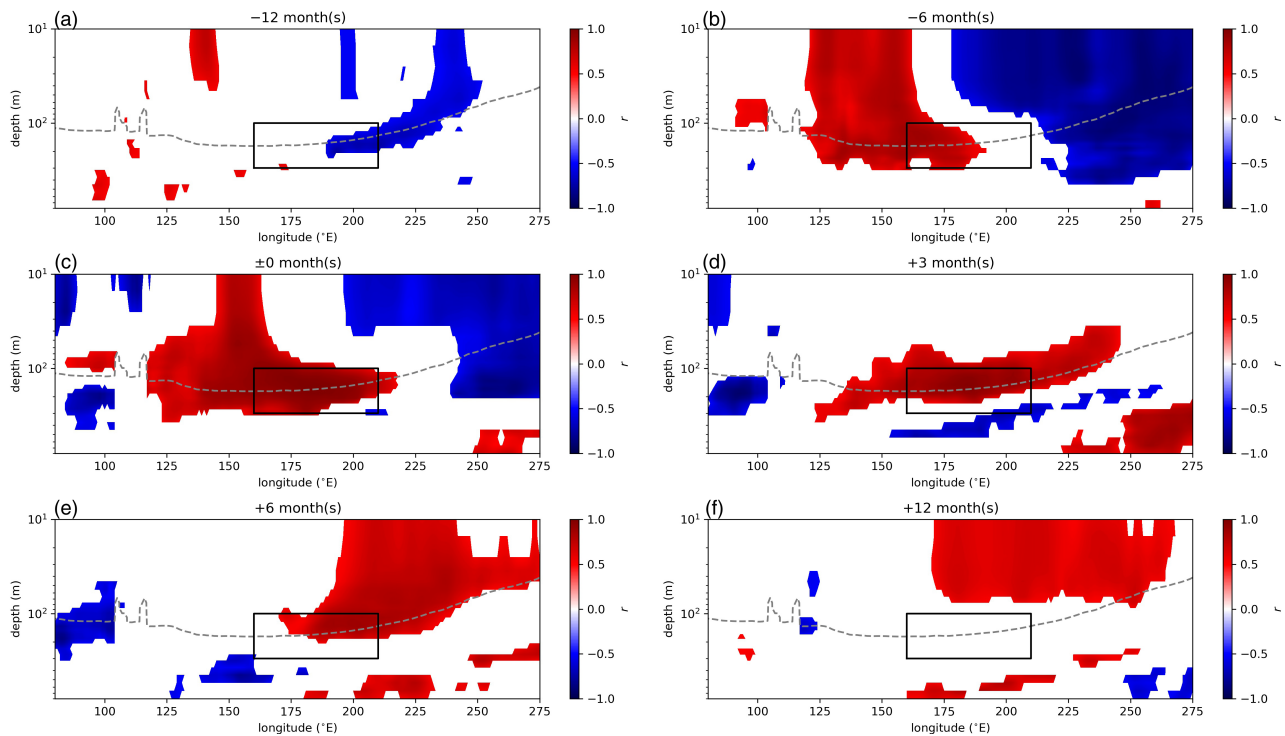


FIGURE 3 Similar to Figure 2, but showing correlation ($p < 0.05$) between the SubNiño4 index and SubT profile averaged between 5°S and 5°N with various lead/lag times from the peak of subsurface warm/cold events [Colour figure can be viewed at wileyonlinelibrary.com]

index is significantly correlated with the Niño 3.4 index over the main season. This long-range correlation is robust across the four main seasons and various lead times, with the correlation coefficient generally staying above 0.4. The correlation between the WWV_W anomaly and Niño 3.4 is less robust, especially at shorter lead times. It is, however, similar to SubNiño4 at time-scales of about one year. Not only does this show that SubT anomalies in the equatorial West Pacific precede SST anomalies further east, confirming the delayed connection between the subsurface and surface temperature anomalies hinted at in Figure 1a and observed in the generic deseasonalised cycle shown in Figures 2 and 3, but it also suggests that the SubNiño4 index is a simple indicator more robust with time than the WWV_W anomaly for ENSO and hence atmospheric phenomena driven by it. We find very similar correlations for SubNiño4 with Niño 3, Niño 3.4, and Niño 4 (e.g., 0.40, 0.46, and 0.48, respectively at 12 months lead time for DJF).

3.2 | Delayed teleconnections of SubNiño4

3.2.1 | Regional precipitation

The lagged correlation maps between precipitation in the four main seasons and the SubNiño4 index one year ahead

of each are shown in Figure 5. The most conspicuous feature is the year-round anticorrelation over Southeast Asia. There is also a clear anticorrelation signal during the boreal spring (MAM) in Northeast Brazil extending eastwards into the Atlantic.

Figures 6–10 show the lagged correlation coefficients (r^2) between various regional precipitation values and the Niño 3.4 and SubNiño4 indices and the WWV_W anomaly, to better exhibit, by removing the sign, the handover of significant correlation with precipitation from the subsurface to the surface. Corresponding plots showing the correlation coefficients without squaring are provided as supporting information (Figures S2–S6).

Figure 6 shows the correlation coefficients (r^2) between the precipitation over the Maritime Continent in the four main seasons and the Niño 3.4 and SubNiño4 indices and WWV_W anomaly in the 25 overlapping three-month periods leading to the main seasons. SubNiño4 becomes significantly correlated with precipitation much earlier than Niño 3.4. The correlations between SubNiño4 around 6–12 months ahead and precipitation in all four main seasons stand at a level of around -0.4 . The WWV_W anomaly in general gives weaker correlations than SubNiño4 with precipitation in all four main seasons. It fails to correlate significantly with precipitation in MAM, while in the other three main seasons significance is sustained over a much smaller window of lead times compared with SubNiño4. Meanwhile, the simultaneous

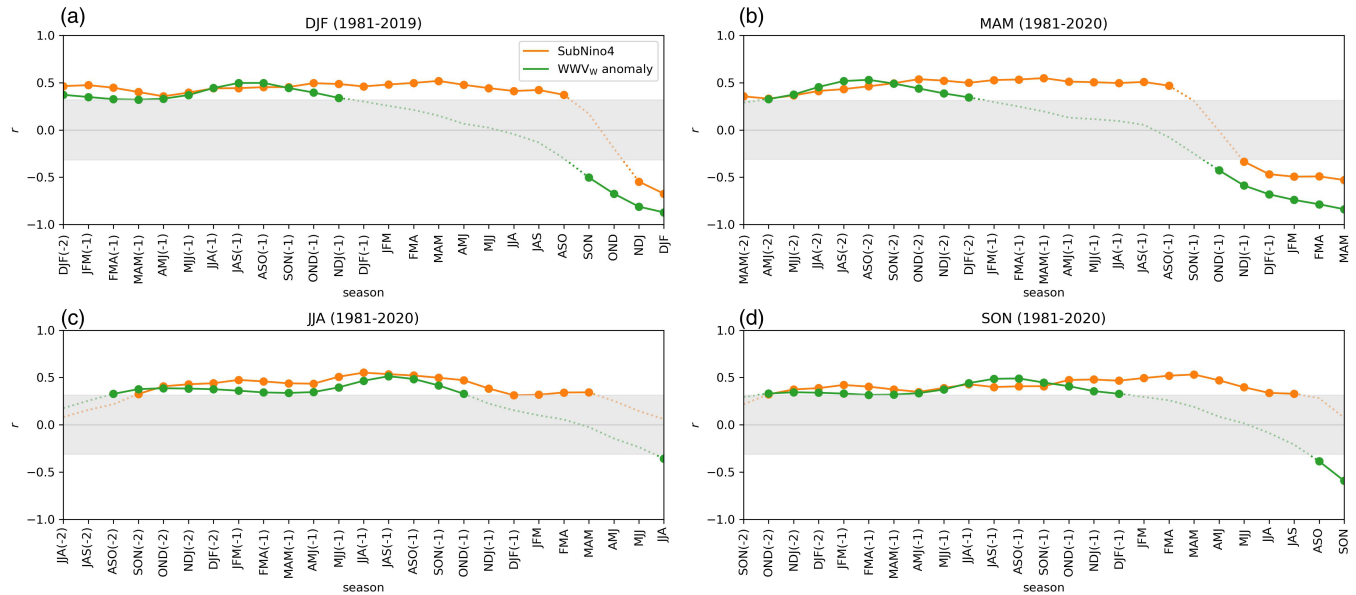


FIGURE 4 (a) Correlation, r , between Niño 3.4 in DJF and SubNiño4 (orange) and the WWV_w anomaly (green) in the 25 overlapping three-month periods immediately prior. (b) Same as (a) but for MAM. (c) Same as (a) but for JJA. (d) Same as (a) but for SON. (a–d) Correlations with $p < 0.05$ are indicated with solid dot markers and connected with a solid line. Grey shading indicates correlation levels with $p \geq 0.05$ [Colour figure can be viewed at wileyonlinelibrary.com]

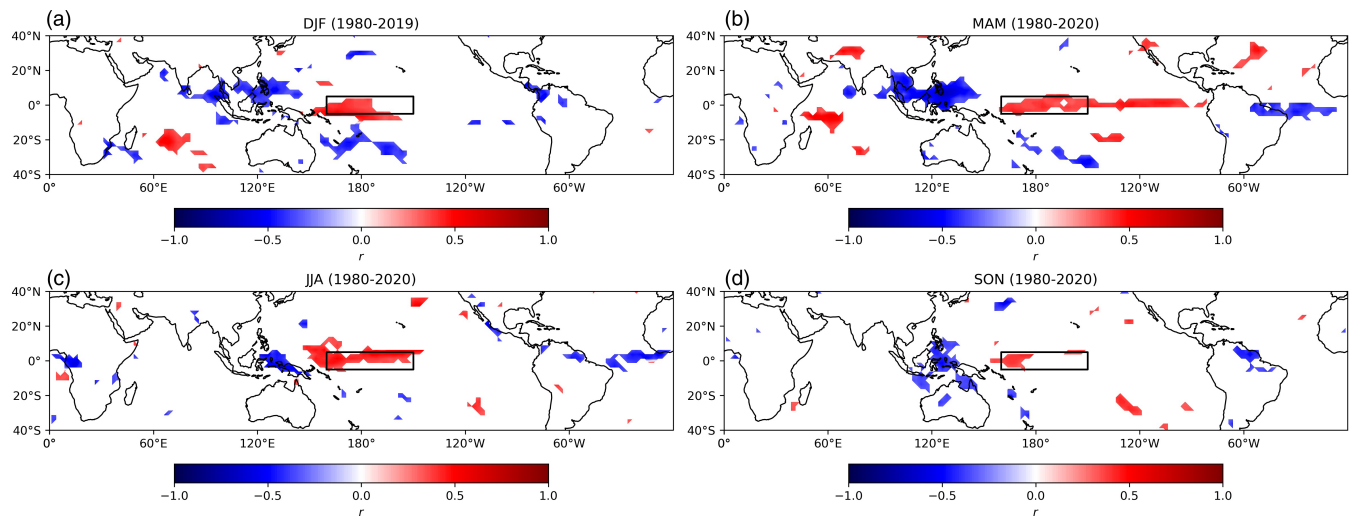


FIGURE 5 (a) Correlation ($p < 0.05$) between precipitation in DJF and the SubNiño4 index 12 months prior. (b) Same as (a) but for MAM. (c) Same as (a) but for JJA. (d) Same as (a) but for SON. (a–d) The black box indicates the extent of the SubNiño4 region [Colour figure can be viewed at wileyonlinelibrary.com]

correlations between Niño 3.4 and precipitation in DJF, JJA, and SON all go beyond $r = -0.81$ ($p < 0.01$) while that in MAM is at $r = -0.52$ ($p < 0.01$). The simultaneous correlation with Niño 3.4 in MAM is particularly low compared with those in the other three main seasons, while the lagged correlations with SubNiño4 are similar across the four main seasons and are least robust in SON.

Figure 7 shows the correlation coefficients (r^2) between precipitation over Northeast Brazil and South

Africa in MAM and DJFM respectively and the Niño 3.4 and SubNiño4 indices and WWV_w anomaly in the 25 overlapping three-month periods leading to the precipitation seasons considered. In both cases, SubNiño4 becomes significantly correlated with precipitation around 15 months ahead of the relevant precipitation season, half a year earlier than Niño 3.4. At long lead times, the WWV_w anomaly is significantly correlated with precipitation over Northeast Brazil in MAM from nearly two years earlier,

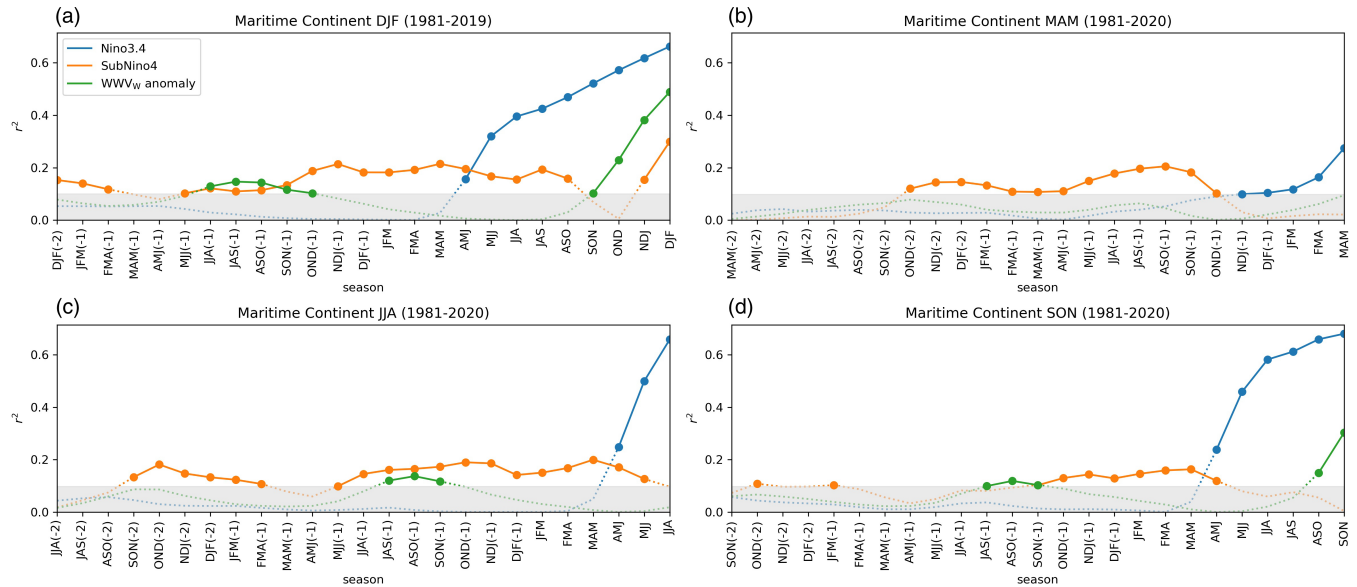


FIGURE 6 (a) Correlation, r^2 , between Maritime Continent precipitation in DJF and SubNiño4 (orange), WWV_w anomaly (green), and Niño 3.4 (blue) in the 25 overlapping three-month periods immediately prior. (b) Same as (a) but for MAM. (c) Same as (a) but for JJA. (d) Same as (a) but for SON. (a–d) Correlations with $p < 0.05$ are indicated with solid dot markers and connected with solid lines. Grey shading indicates correlation levels with $p \geq 0.05$ [Colour figure can be viewed at wileyonlinelibrary.com]

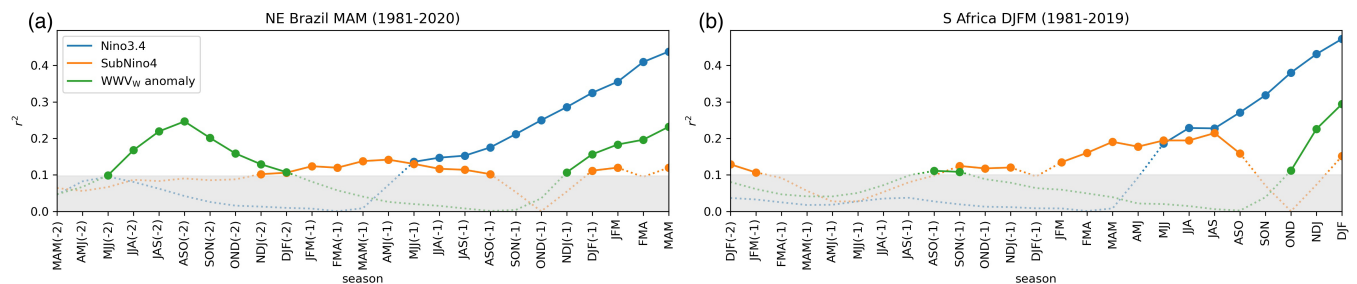


FIGURE 7 (a) Same as Figure 6a but for Northeast Brazil precipitation in MAM. (b) Same as (a) but for South Africa precipitation in DJFM [Colour figure can be viewed at wileyonlinelibrary.com]

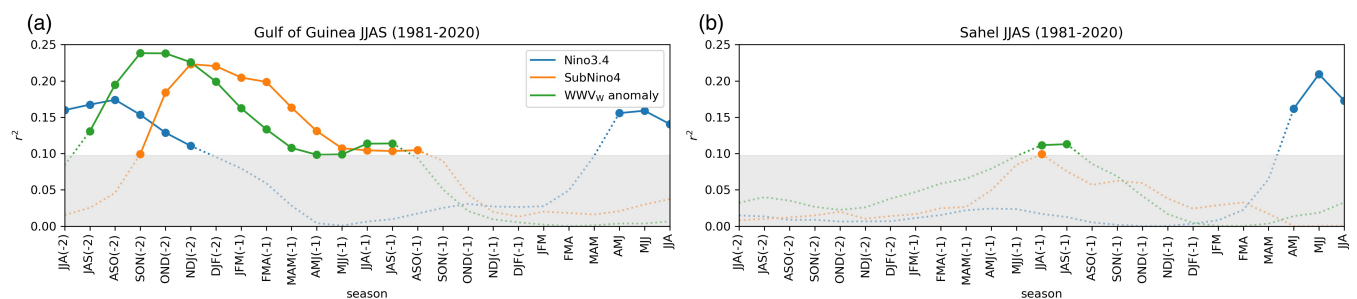


FIGURE 8 (a) Same as Figure 6a, but for Gulf of Guinea precipitation in JAS. (b) Same as (a), but for Sahel precipitation [Colour figure can be viewed at wileyonlinelibrary.com]

but then SubNiño4 has stronger correlations at around one year's lead. Only SubNiño4 shows robust significant correlation with precipitation over South Africa in DJFM. The simultaneous correlations between Niño 3.4 and

precipitation in Northeast Brazil and South Africa are $r = -0.66$ ($p < 0.01$) and $r = -0.69$ ($p < 0.01$) respectively, while the lagged correlations with SubNiño4 around a year ahead stand at a level of about -0.35 .

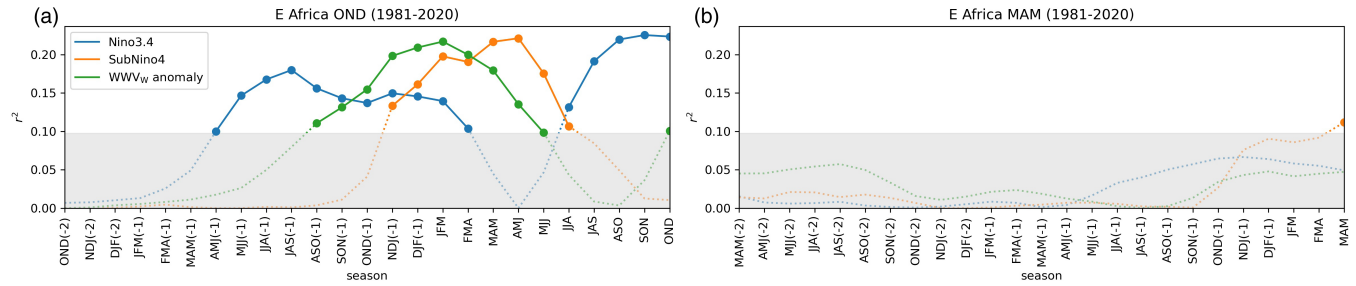


FIGURE 9 (a) Same as Figure 6a, but for East Africa precipitation in OND. (b) Same as (a), but for MAM [Colour figure can be viewed at wileyonlinelibrary.com]

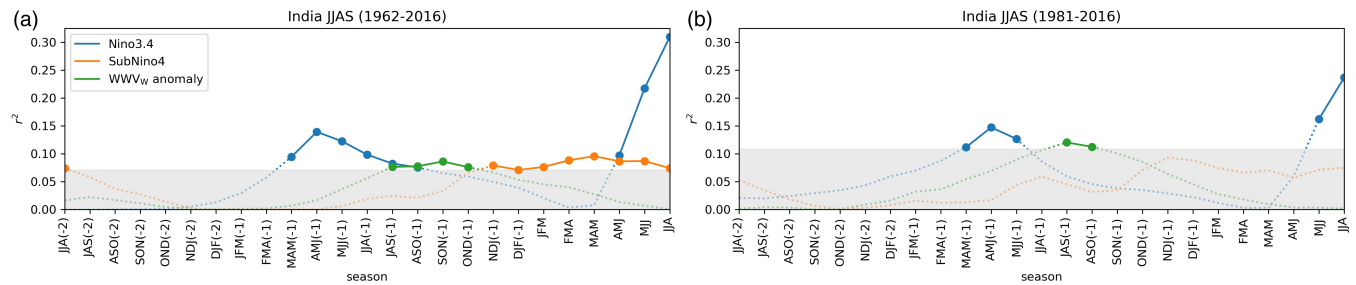


FIGURE 10 (a) Same as Figure 6a, but for India precipitation in JJAS computed with data from 1960–2016. (b) Same as (a), but computed with data from 1979–2016 [Colour figure can be viewed at wileyonlinelibrary.com]

Figure 8 shows the correlation coefficients (r^2) between the precipitation over two regions in West Africa—the Gulf of Guinea and Sahel—in JJAS and the Niño 3.4 and SubNiño4 indices and WWV_w anomaly in the 25 overlapping three-month periods leading to the precipitation season considered. In both regions, Niño 3.4 becomes significantly correlated with precipitation in JJAS two months ahead and remains at a level of around -0.4 . Interestingly, for the Gulf of Guinea, the precipitation is also significantly correlated with Niño 3.4 more than 19 months ahead at a level of around 0.4 . Precipitation over the Gulf of Guinea shows significant correlation with SubNiño4 10–21 months ahead, ranging from $r = -0.32$ ($p < 0.05$) to $r = -0.47$ ($p < 0.01$). The correlation pattern with the WWV_w anomaly is similar to that of SubNiño4, but shifted earlier by two months. Meanwhile, the precipitation over Sahel does not show robust significant correlation with either SubNiño4 or the WWV_w anomaly.

Figure 9 shows the correlation coefficients (r^2) between precipitation over East Africa during the so-called short rains (OND) and long rains (MAM) seasons and the Niño 3.4 and SubNiño4 indices and WWV_w anomaly in the 25 overlapping three-month periods leading to the two precipitation seasons. For the short rains season, the simultaneous correlation between precipitation and Niño 3.4 is $r = 0.47$ ($p < 0.01$). The precipitation also shows significant correlation with SubNiño4 4–11 months ahead, ranging from $r = 0.33$ ($p < 0.05$) to $r = 0.47$

($p < 0.01$), and with Niño 3.4 8–18 months ahead, ranging from $r = -0.32$ ($p < 0.05$) to $r = -0.42$ ($p < 0.01$). The correlation pattern with the WWV_w anomaly is similar to that of SubNiño4 but shifted earlier by two months. On the other hand, there are no robust significant correlations between long rains season precipitation and either Niño 3.4, SubNiño4, or the WWV_w anomaly.

Figure 10 shows the correlation coefficients (r^2) between the precipitation over India in JJAS and the Niño 3.4 and SubNiño4 indices and WWV_w anomaly in the 25 overlapping three-month periods leading to the precipitation season considered, computed using data from 1960–2016 (Figure 10a) and 1979–2016 (Figure 10b). Since the IITM–IMR dataset is only available up to 2016, it is not possible to keep the same period of study as for the other regional precipitation. With data from 1960–2016, the simultaneous correlation between precipitation and Niño 3.4 is $r = -0.56$ ($p < 0.01$). The precipitation also shows significant correlation with SubNiño4 0–7 months, ahead ranging from $r = -0.27$ ($p < 0.05$) to $r = -0.31$ ($p < 0.05$) and with Niño 3.4 10 to 15 months ahead ranging from $r = 0.27$ ($p < 0.05$) to $r = 0.37$ ($p < 0.01$). The WWV_w anomaly gives significant correlation with precipitation at lead times of around 10 months. With data from 1979–2016, the simultaneous correlation between precipitation and Niño 3.4 is slightly lower ($r = -0.47$, $p < 0.01$). The correlations with SubNiño4, however, are similar to those computed with data from 1960–2016. Nonetheless,

they are not deemed statistically significant, mostly due to a reduction in sample size.

In general, for all cases where there is significant simultaneous correlation between precipitation and Niño 3.4, except for Sahel JJAS, the correlations between precipitation and SubNiño4 become significant before Niño 3.4; as we move closer to the precipitation seasons considered, correlations with Niño 3.4 kick in, while those with SubNiño4 fade. Around 6–12 months (or even further into the past) prior to the precipitation seasons considered, correlations with SubNiño4 are significant but not those with Niño 3.4. The WWV_w anomaly gives weaker, less robust, and less reliable correlation with precipitation overall. It leads earlier than SubNiño4 in some cases but can fail completely for some others. For consistency, we present results for precipitation regions and seasons based on, if not taken directly from, previous studies. We note here that both the regions and seasons could be fine-tuned further to achieve higher correlations with both surface and subsurface signals. Here our intention is to confirm the existence of basic robust relationships.

3.2.2 | Fires in Southeast Asia

We next explore the relationship of SubNiño4 with fire, which has high impact and is partially linked to precipitation. Figure 11a shows the average annual fire count from 2001–2018 over Southeast Asia. Continental and Maritime Southeast Asia, with most of the fire captured by the red and purple boxes respectively, have distinct fire seasonal cycles. Since MODIS fire data only cover from 2001–2018, to keep the period of study the same as that for precipitation, we rely on the FWI, a fire-risk index, produced from ERA5 data. The FWI seasonal cycles of Continental and Maritime Southeast Asia peak in DJFM and July–October (JASO), respectively. For the period when both MODIS and FWI data are available, the fire count and FWI are highly correlated: for Continental Southeast Asia (DJFM), $r = 0.88$, $p < 0.01$ ($r = 0.84$, $p < 0.01$); for Maritime Southeast Asia (JASO), $r = 0.89$, $p < 0.01$ ($r = 0.96$, $p < 0.01$).

Figure 11b,c shows the correlation coefficients (r^2) between the FWI for Continental and Maritime Southeast Asia in DJFM and JASO respectively and the Niño 3.4 and SubNiño4 indices and WWV_w anomaly in the 25 overlapping three-month periods leading to the fire seasons considered. Here, r^2 is again shown to exhibit more clearly the handover of significant correlation from the subsurface to the surface than showing r as in the Supporting Information (Figure S7). For Continental Southeast Asia, the simultaneous correlation between Niño 3.4 and FWI in DJFM is $r = 0.53$ ($p < 0.01$). The FWI also shows significant correlation with SubNiño4 4–19 months ahead,

ranging from $r = 0.32$ ($p < 0.05$) to $r = 0.44$ ($p < 0.01$), and with the WWV_w anomaly at lead times of around 18 months at a lower level overall. For Maritime Southeast Asia, the simultaneous correlation between Niño 3.4 and FWI in JASO is $r = 0.77$ ($p < 0.01$). The FWI also shows significant correlation with SubNiño4 2–20 months ahead, ranging from $r = 0.31$ ($p < 0.05$) to $r = 0.45$ ($p < 0.01$) with a break at 14 and 15 months ahead, and with the WWV_w anomaly 10 to 12 months ahead, again at a lower level overall. Although the simultaneous correlation between Niño 3.4 and FWI for Maritime Southeast Asia JASO is much higher than that for Continental Southeast Asia DJFM, the lagged correlations with SubNiño4 for the FWI in both cases are at a similar level.

4 | DISCUSSION

The SubNiño4 index, Niño4–Z20 anomaly, and WWV_w anomaly are essentially measures of the same state of the ENSO cycle capturing the essential feature of the recharge cycle, specifically in the subsurface equatorial West Pacific on longer time-scales. Izumo *et al.* (2019) showed that the variability of this state is primarily a consequence of wind-forced slow Rossby waves. We see from Figure 1a that the SubNiño4 index leads the Niño 3.4 index. This is consistent with the lead relationship between the thermocline and surface ENSO variabilities established through, for example, studies of WWV_w (Ballester *et al.*, 2016; Izumo *et al.*, 2019). Figure 1a also shows that there is interdecadal variability in the relationship. The amplitude of the SubNiño4 index is much reduced post-2000, especially for cold anomalies, and has become less periodic compared with pre-2000. Furthermore, after 2000 the warm/cold events on the surface follow those in the subsurface less closely than before, as reported previously by Zhao *et al.* (2021).

Composite analysis of subsurface warm and cold episodes (Figures 2 and 3) reveals how the subsurface temperature anomalies evolve to become surface temperature anomalies after around 6–12 months. The evolution of the subsurface temperature anomalies we observed following subsurface warm/cold episodes is consistent with that during a generic ENSO cycle, as reported by others (e.g., Timmermann *et al.*, 2018; Lin and Qian, 2019). Such delayed connection between the subsurface and surface temperature anomalies is confirmed by correlation analysis between the SubNiño4 and Niño 3.4 indices shown in Figure 4 and appears to be a robust year-round feature. Figure 4 also shows that the SubNiño4 index correlations are more stable with lead time than the widely used WWV_w. In particular, they decrease much less quickly at shorter lead times than WWV_w. A further merit of the

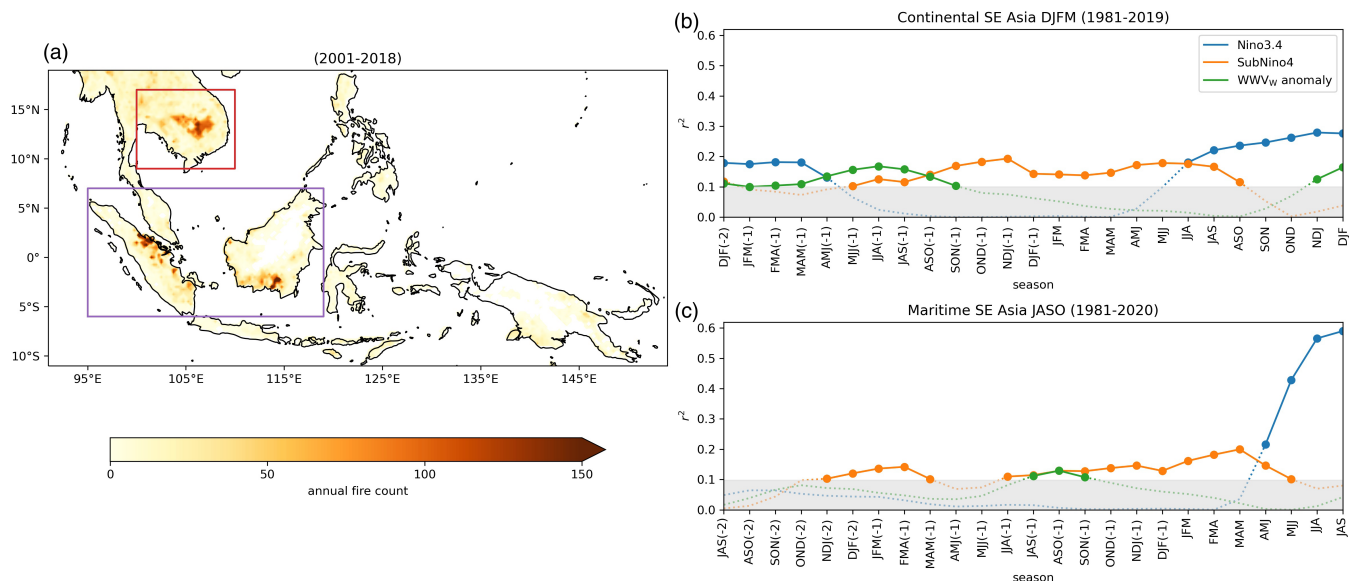


FIGURE 11 (a) Annual mean fire count over Southeast Asia. The red and purple boxes are for Continental and Maritime Southeast Asia respectively. (b) Same as Figure 6a but for Continental Southeast Asia FWI in DJFM. (c) Same as (b) but for Maritime Southeast Asia FWI in JASO [Colour figure can be viewed at [wileyonlinelibrary.com](https://onlinelibrary.wiley.com)]

SubNiño4 index, or alternatively Niño4–Z20, over WWVW is that, unlike the latter, the (Sub)Niño4 region is completely free of land, making it more directly relevant to the ocean dynamics. The SubNiño4 index, or Niño4–Z, is a practical and stable index that captures well-known ENSO physics and can serve as a long-range indicator of surface ENSO and thus atmospheric phenomena driven by it.

The Fourier spectrum we obtained for the Niño 3.4 index (Figure 1b) is consistent with that in Petrova *et al.* (2017) for Niño 3.4 and those in Latif *et al.* (1998) and Rasmusson and Carpenter (1982) for Niño 3. The dominant quasi-quadrennial peak and the secondary quasi-biennial peak are well-established features also present in our SubNiño4 spectrum. The SubNiño4 index may be less noisy than the Niño 3.4 index because of a lack of direct atmospheric coupling of the subsurface compared with the surface, making SubT less prone to influences from high-frequency or stochastic atmospheric forcings than the SST. The normalised histogram of the SubNiño4 index resembles that of the Niño4–Z20 anomaly (Figure 1c,d); the two have similar negative skewness and are essentially interchangeable variables ($r = 0.99$, $p < 0.01$), effectively being equivalent measures of the thermocline–mixed-layer interface. The surface zonal wind stress anomaly over the Niño 4 region is positively skewed, with lower absolute skewness than the SubNiño4 index, and is significantly correlated with it in December and January only. The reason why the SubNiño4 index displays such pronounced (negative) skewness not exhibited by the Niño 3.4 index is unclear to us, but the skewed surface zonal wind stress anomaly (Planton *et al.*, 2018)

and subsurface nonlinear dynamical heating (e.g., Hayashi *et al.*, 2020) may be contributing factors. Izumo *et al.* (2019) also noted the importance of multimonth integrated wind forcing, rather than just considering single-month correlations.

Dynamical ENSO predictions show both interdecadal (Barnston *et al.*, 2012; Zhang *et al.*, 2021) and seasonal (Jin *et al.*, 2008; Barnston *et al.*, 2012; Sun *et al.*, 2018) variations in predictive skill and different models are not always available at lead times of more than 12 months. For those that are, the typical correlation skill is at the level of 0.5 on average for 12-month forecasts. At such a long lead time, ENSO correlation with the lead observed SubNiño4 index (Figure 4) is on par with the simultaneous correlation from typical dynamical predictions. Together with the established ocean heat content advective processes necessary for the onset of El Niño (Ramesh and Murtugudde, 2013; Ballester *et al.*, 2016; Timmermann *et al.*, 2018), this confirms that initialisation of the equatorial Pacific SubT profile is a major source of long-range ENSO predictive skill from dynamical models. The importance of the equatorial Pacific thermocline has been demonstrated by data assimilation and ensemble prediction methods that target optimal equatorial Pacific subsurface temperature disturbances for dynamical ENSO prediction (e.g., Yang *et al.*, 2008; O’kane *et al.*, 2019). Furthermore, predictions of ENSO-driven atmospheric phenomena at such lead times afforded by the observed SubNiño4 index can be expected to be no worse than those by predicated SST from dynamical models. Takaya *et al.* (2021) demonstrated skilful long-range dynamical large ensemble monsoon

predictions. They attributed the skill to SST anomalies and did not explore further the role of the Pacific subsurface that we highlight here. It could be that their subsurface initialisation is the dominant factor for their long-range skill. Here we demonstrated the potential of the SubNiño4 index by finding robust lagged correlations with regional precipitation and fires. To evaluate its performance directly against the dynamically predicted ENSO, we suggest comparing the mutual information between the atmospheric response to predicted and lead observed SubNiño4 and simultaneous dynamically predicted Niño 3.4 respectively, provided that time series of predicted Niño 3.4 are available. This reveals the amount of information about the atmospheric response to be predicted that can be learnt from the two predictors respectively.

ENSO's effects on precipitation have been studied on a global scale in detail by Lenssen *et al.* (2020), Davey *et al.* (2014), Ropelewski and Halpert (1987), Ropelewski and Halpert (1989), and Kiladis and Diaz (1989), for example. They mapped out regions around the globe where the precipitation over various time windows is correlated strongly and coherently with ENSO. While we do not aim, nor can we expect, that our correlation analysis with global precipitation over the four main seasons and SubNiño4 with a very long lead time of 12 months (Figure 5) will reproduce exactly the patterns identified by, say, Lenssen *et al.* (2020), it suggests that the SubNiño4 index has strong potential as a long-range predictor for ENSO-driven precipitation.

The effects of ENSO on precipitations on a regional level have also been extensively studied. Some of the regions and seasons where ENSO is known to play an important role in interannual precipitation variability are summarised as follows. Over the Maritime Continent, the precipitation and ENSO signal are anticorrelated throughout the year (As-Syakur *et al.*, 2016; Yanto *et al.*, 2016; King and Vincent, 2018); in Northeast Brazil, the precipitation and ENSO signal are anticorrelated in the wet season (MAM, see Folland *et al.*, 2001; Andreoli and Kayano, 2006); in West Africa, the precipitation and ENSO signal are anticorrelated in the wet season (JJAS, see Losada *et al.*, 2012; Srivastava *et al.*, 2019); in South Africa, the precipitation and ENSO signal are anticorrelated in the wet season (DJFM, see Yuan *et al.*, 2014; Hoell *et al.*, 2017); in East Africa, the precipitation and ENSO signal are positively correlated in the so-called short rains season (OND) but have insignificant correlation in the so-called long rains season (MAM, see Mutai *et al.*, 1998; Vigaud *et al.*, 2017; Vellinga and Milton, 2018; Park *et al.*, 2020).

The simultaneous correlations between Niño 3.4 and precipitation from our analysis agree with all these reported ENSO–precipitation relationships. The lagged correlations between SubNiño4 and precipitation have

the same sign as the simultaneous correlations with Niño 3.4. As expected, the long-range correlation is generally smaller than that in-season, but it is significant over many lead times. In some cases, the long-range correlation is even as large as the in-season correlation.

It is worth noting that, for the Maritime Continent, while the simultaneous correlation with Niño 3.4 in MAM is particularly lower than those in the other three main seasons, consistent with the northwards shift in ENSO influence in the region observed by As-Syakur *et al.* (2016), the lagged correlations with SubNiño4 are similar throughout the year and least robust in SON. For West Africa JJAS, although the simultaneous correlations with Niño 3.4 for both the Gulf of Guinea and Sahel are similar, the SubNiño4 index as an indicator is much more reliable and robust for the Gulf of Guinea than Sahel. Although the correlation analysis performed by Losada *et al.* (2012) employed Niño 3 and their period of study stopped just before ours, the simultaneous correlations between Niño 3.4 and precipitation in the Gulf of Guinea and Sahel from our study agree with the values towards the end of their study period. Losada *et al.* (2012) used a Monte Carlo test to determine significance and, interestingly, towards the end of their study period, although the correlations between Niño 3 and precipitation in the Gulf of Guinea and Sahel are at the same level, only the former was deemed significant. As for East Africa, significant simultaneous (lagged) correlations with Niño 3.4 (SubNiño4) are observed for the short rains season (OND) but not for the long rains season (MAM) as expected, indicating that the SubNiño4 index correlates only when there is also significant simultaneous correlation with Niño 3.4.

The correlation patterns of fire with Niño 3.4 and SubNiño4 resemble those of precipitation. This verifies that the SubNiño4 index is useful as an indicator not just of precipitations but also other ENSO-driven anomalies in general. Sparks and Toumi (2020) originally proposed the subsurface heat content to be a predictor of South China tropical cyclone landfall, because the index can anticipate changes in the steering-level winds. SubNiño4 as a long-range predictor is therefore of potential interest for a broad range of atmospheric phenomena.

The domains and seasons we chose to study Southeast Asia fires do not correspond exactly to those used to study Maritime Continent precipitation. In particular, Maritime Southeast Asia represents only a small part of the Maritime Continent and Continental Southeast Asia is completely separate from the Maritime Continent. Nonetheless, the correlation patterns for fires in both cases appear to be consistent with those for precipitation. Maritime Southeast Asia fires are known to be strongly driven by local precipitation and ENSO (Wooster *et al.*, 2012; Liew, 2013;

Fanin and Van Der Werf, 2017). However, there is a lack of literature on the relations between Continental Southeast Asia fires, local precipitation, and ENSO. In a global study on burnt-area forecast with SST by Chen *et al.* (2016), among the 14 ocean climate indices considered, ENSO-related ones are optimal for correlation with the annual burnt area of six out of 12 hotspot regions identified. However, their clustering algorithm failed to capture the most severely burnt region in Continental Southeast Asia. Our study suggests that ENSO also plays a role in the regulation of fire activity over Continental Southeast Asia.

Compared with the SubNiño4 index, correlations of the WVW_W anomaly with the Niño3.4 index are similar in strength and have similar long lead times, but are less well sustained into shorter lead times. The SubNiño4 index, Niño4–Z20 anomaly, and WVW_W anomaly all essentially capture of the same state of the ENSO cycle. We are not proposing any novel fundamental aspects about the dynamics of ENSO. However, the SubNiño4 index has temporally more stable and sustained, and at times stronger, correlations with the Niño3.4 index, while covering a smaller domain compared with the WVW_W anomaly. It may identify more precisely the critical point of action of the subsurface branch of established ENSO dynamics.

We study in detail for the first time the implications of the subsurface temperature anomaly on atmospheric anomalies, in particular regional precipitation throughout the Tropics and fires in Southeast Asia. The correlations of the WVW_W anomaly with the regional precipitation and fire investigated are overall weaker, less robust, and sustained over a narrower window of lead times compared with the SubNiño4 index. In a few cases, the correlation patterns resemble those of SubNiño4 but with a slight shift towards longer lead times. This is consistent with the eastwards propagation of the SubT anomaly in the equatorial Pacific and the WVW_W region being centred westwards of the (Sub)Niño4 region. In many of the other cases, the WVW_W anomaly is less correlated with regional precipitation and fire over a smaller time window compared with SubNiño4. Sometime the WVW_W anomaly does not work at all when the SubNiño4 index is still a useful indicator. The utility of the WVW_W anomaly may also be limited, because its domain of definition is problematic, as it includes considerable land mass to the west. The (Sub)Niño4 region does not have this issue.

5 | CONCLUSIONS

We extend the SubNiño4 index originally proposed by Sparks and Toumi (2020) and give it a fuller investigation, revealing its relation to the surface Niño indices. We

show that the SubNiño4 index captures the evolution of subsurface ocean heat content between the El Niño and La Niña phases of the ENSO cycle, thus allowing it to serve as a long-range indicator of Niño 3.4 and ENSO-driven atmospheric phenomena. It achieves this with temporally more stable correlations compared with the commonly used WVW_W anomaly. We demonstrate that the ENSO correlation with the SubNiño4 index matches that of the WVW_W anomaly and becomes significant at around the same lead time. However, the SubNiño4 correlation is sustained further into shorter lead times. At lead times of the order of 12 months, observed Niño 3.4 correlations with the lead observed SubNiño4 index become similar to and can exceed those produced with typical dynamical model ENSO predictions. Our study confirms that an important source of long-range predictive skill for ENSO in dynamical models can be understood to stem from good initialisation of the subsurface temperature profile in the western equatorial Pacific. We further establish the potential value and viability of the SubNiño4 index as a long-range indicator of atmospheric phenomena driven by ENSO, particularly regional precipitation anomalies throughout the Tropics and fires in Continental and Maritime Southeast Asia.

AUTHOR CONTRIBUTIONS

Enoch Yan Lok Tsui: conceptualization; data curation; formal analysis; investigation; methodology; software; validation; visualization; writing – original draft; writing – review and editing. **Ralf Toumi:** conceptualization; formal analysis; funding acquisition; investigation; methodology; project administration; resources; supervision; validation; writing – review and editing.

ACKNOWLEDGEMENTS

This research was funded by the Leverhulme Centre for Wildfires, Environment and Society through the Leverhulme Trust, grant number RC-2018-023, NERC/UKRI NE/V017756/1 and the Singapore Green Finance Centre. The authors thank Nathan Sparks for the computation of the Z20 profile from the SubT data.

The authors made the following contributions: E.Y.L.T.—conceptualisation, data curation, formal analysis, investigation, methodology, software, validation, visualisation, writing (original draft, review, and editing); R.T.—conceptualisation, formal analysis, funding acquisition, investigation, methodology, projection administration, resources, supervision, validation, writing (review and editing).

CONFLICT OF INTERESTS

The authors declare no conflict of interests.

ORCID

Enoch Yan Lok Tsui  <https://orcid.org/0000-0003-1621-0443>

REFERENCES

- Adler, R., Wang, J.-J., Sapiiano, M., Huffman, G., Chiu, L., Xie, P.P., Ferraro, R., Schneider, U., Becker, A., Bolvin, D., Nelkin, E., Gu, G. and Program, N.C. (2016) *Global Precipitation Climatology Project (GPCP) Climate Data Record (CDR), Version 2.3 (Monthly)*. National Centers for Environmental Information.
- Andreoli, R.V. and Kayano, M.T. (2006) Tropical Pacific and south Atlantic effects on rainfall variability over northeast Brazil. *International Journal of Climatology*, 26(13).
- As-Syakur, A.R., Osawa, T., Miura, F., Nuarsa, I.W., Ekayanti, N.W., Dharma, I.G.B.S., Adnyana, I.W.S., Arthana, I.W. and Tanaka, T. (2016) Maritime Continent rainfall variability during the TRMM era: the role of monsoon, topography and El Niño Modoki. *Dynamics of Atmospheres and Oceans*, 75.
- Ballester, J., Bordoni, S., Petrova, D. and Rodó, X. (2016) Heat advection processes leading to El Niño events as depicted by an ensemble of ocean assimilation products. *Journal of Geophysical Research: Oceans*, 121(6).
- Barnston, A.G., Tippett, M.K., L'Heureux, M.L., Li, S. and Dewitt, D.G. (2012) Skill of real-time seasonal ENSO model predictions during 2002–11: is our capability increasing?. *Bulletin of the American Meteorological Society*, 93(5).
- Battisti, D.S. and Hirst, A.C. (1989) Interannual variability in a tropical atmosphere–ocean model: influence of the basic state, ocean geometry and nonlinearity. *Journal of the Atmospheric Sciences*, 46(12).
- Bjerknes, J. (1969) Atmospheric teleconnections from the equatorial Pacific. *Monthly Weather Review*, 97(3).
- Chen, Y., Morton, D.C., Andela, N., Giglio, L. and Randerson, J.T. (2016) How much global burned area can be forecast on seasonal time scales using sea-surface temperatures?. *Environmental Research Letters*, 11(4).
- Davey, M.K., Brookshaw, A. and Ineson, S. (2014) The probability of the impact of ENSO on precipitation and near-surface temperature. *Climate Risk Management*, 1.
- Di Giuseppe, F., Pappenberger, F., Wetterhall, F., Krzeminski, B., Camia, A., Libertá, G. and Miguel, J.S. (2016) The potential predictability of fire danger provided by numerical weather prediction. *Journal of Applied Meteorology and Climatology*, 55(11).
- Drosowsky, W. (2006) Statistical prediction of ENSO (Nino 3) using sub-surface temperature data. *Geophysical Research Letters*, 33(3).
- European Centre for Medium-Range Weather Forecasts (2019) *Fire danger indices historical data from the Copernicus Emergency Management Service*. Copernicus Climate Change Service (C3S) Climate Data Store (CDS). 10.24381/cds.0e89c522.
- Fanin, T. and Van Der Werf, G.R. (2017) Precipitation–fire linkages in Indonesia (1997–2015). *Biogeosciences*, 14(18).
- Folland, C.K., Colman, A.W., Rowell, D.P. and Davey, M.K. (2001) Predictability of northeast Brazil rainfall and real-time forecast skill, 1987–98. *Journal of Climate*, 14(9).
- Giglio, L., Csiszar, I. and Justice, C.O. (2006) Global distribution and seasonality of active fires as observed with the Terra and Aqua moderate resolution imaging spectroradiometer (MODIS) sensors. *Journal of Geophysical Research: Biogeosciences*, 111(2).
- Giglio, L., Schroeder, W., Hall, J.V. and Justice, C.O. (2020). MODIS Collection 6 Active Fire Product User's Guide Revision C. https://modis-fire.umd.edu/files/MODIS_C6_Fire_User_Guide_C.pdf.
- Giglio, L., Schroeder, W. and Justice, C.O. (2016) The collection 6 MODIS active fire detection algorithm and fire products. *Remote Sensing of Environment*, 178.
- Good, S.A., Martin, M.J. and Rayner, N.A. (2013) EN4: quality controlled ocean temperature and salinity profiles and monthly objective analyses with uncertainty estimates. *Journal of Geophysical Research: Oceans*, 118(12).
- Gouretski, V. and Cheng, L. (2020) Correction for systematic errors in the global dataset of temperature profiles from mechanical bathythermographs. *Journal of Atmospheric and Oceanic Technology*, 37(5).
- Gouretski, V. and Reseghetti, F. (2010) On depth and temperature biases in bathythermograph data: Development of a new correction scheme based on analysis of a global ocean database. *Deep-Sea Research Part I: Oceanographic Research Papers*, 57(6).
- Hayashi, M., Jin, F.F. and Stuecker, M.F. (2020) Dynamics for El Niño–La Niña asymmetry constrain equatorial-Pacific warming pattern. *Nature Communications*, 11(1).
- Hersbach, H., Bell, B., Berrisford, P., Biavati, G., Horányi, A., Muñoz Sabater, J., Nicolas, J., Peubey, C., Radu, R., Rozum, I., Schepers, D., Simmons, A., Soci, C., Dee, D. and Thépaut, J.-N. (2019) *ERA5 monthly averaged data on single levels from 1979 to present*. Copernicus Climate Change Service (C3S) Climate Data Store (CDS). 10.24381/cds.f17050d7.
- Hoell, A., Funk, C., Zinke, J. and Harrison, L. (2017) Modulation of the Southern Africa precipitation response to the El Niño Southern Oscillation by the subtropical Indian Ocean Dipole. *Climate Dynamics*, 48(7–8).
- Izumo, T., Lengaigne, M., Vialard, J., Suresh, I. and Planton, Y. (2019) On the physical interpretation of the lead relation between warm-water volume and the El Niño Southern Oscillation. *Climate Dynamics*, 52(5–6).
- Jin, E.K., Kinter, J.L., Wang, B., Park, C.K., Kang, I.S., Kirtman, B.P., Kug, J.S., Kumar, A., Luo, J.J., Schemm, J., Shukla, J. and Yamagata, T. (2008) Current status of ENSO prediction skill in coupled ocean–atmosphere models. *Climate Dynamics*, 31(6).
- Jin, F.F. (1997a) An equatorial ocean recharge paradigm for ENSO. Part I: conceptual model. *Journal of the Atmospheric Sciences*, 54(7).
- Jin, F.F. (1997b) An equatorial ocean recharge paradigm for ENSO. Part II: a stripped-down coupled model. *Journal of the Atmospheric Sciences*, 54(7).
- Kiladis, G.N. and Diaz, H.F. (1989) Global climatic anomalies associated with extremes in the southern oscillation. *Journal of Climate*, 2(9).
- King, A.D. and Vincent, C.L. (2018) Using global and regional model simulations to understand maritime continent wet-season rainfall variability. *Geophysical Research Letters*, 45(22).
- Kothawale, D.R. and Rajeevan, M. (2017) *Monthly, seasonal and annual rainfall time series for All-India, homogeneous regions and meteorological subdivisions: 1871–2016* Vol. 02. Indian Institute of

- Tropical Meteorology (IITM) Earth System Science Organization, Ministry of Earth Sciences.
- Latif, M., Anderson, D., Barnett, T., Cane, M., Kleeman, R., Leetmaa, A., O'Brien, J., Rosati, A. and Schneider, E. (1998) A review of the predictability and prediction of ENSO. *Journal of Geophysical Research: Oceans*, 103(C7).
- Lenssen, N.J., Goddard, L. and Mason, S. (2020) Seasonal forecast skill of ENSO teleconnection maps. *Weather and Forecasting*, 35(6).
- Liew, S.C. (2013). Anthropogenic and climatic influences on biomass burning in Insular Southeast Asia. In: *International Geoscience and Remote Sensing Symposium (IGARSS)*.
- Lin, J. and Qian, T. (2019) Switch between El Niño and La Niña is caused by subsurface ocean waves likely driven by lunar tidal forcing. *Scientific Reports*, 9(1).
- Losada, T., Rodriguez-Fonseca, B., Mohino, E., Bader, J., Janicot, S. and Mechoso, C.R. (2012) Tropical SST and Sahel rainfall: a non-stationary relationship. *Geophysical Research Letters*, 39(12).
- McGregor, S., Timmermann, A., Schneider, N., Stuecker, M.F. and England, M.H. (2012) The effect of the South Pacific convergence zone on the termination of El Niño events and the meridional asymmetry of ENSO. *Journal of Climate*, 25(16).
- McPhaden, M.J. (2004) Evolution of the 2002/03 El Niño. *Bulletin of the American Meteorological Society*, 85(5).
- Mutai, C.C., Ward, M.N. and Colman, A.W. (1998) Towards the prediction of the East Africa short rains based on sea-surface temperature-atmosphere coupling. *International Journal of Climatology*, 18(9).
- O'kane, T.J., Sandery, P.A., Monselesan, D.P., Sakov, P., Chamberlain, M.A., Matear, R.J., Collier, M.A., Squire, D.T. and Stevens, L. (2019) Coupled data assimilation and ensemble initialization with application to multiyear ENSO prediction. *Journal of Climate*, 32(4).
- Park, S., Kang, D., Yoo, C., Im, J. and Lee, M.I. (2020) Recent ENSO influence on East African drought during rainy seasons through the synergistic use of satellite and reanalysis data. *ISPRS Journal of Photogrammetry and Remote Sensing*, 162.
- Petrova, D., Ballester, J., Koopman, S.J. and Rodó, X. (2020) Multiyear statistical prediction of ENSO enhanced by the tropical Pacific observing system. *Journal of Climate*, 33(1).
- Petrova, D., Koopman, S.J., Ballester, J. and Rodó, X. (2017) Improving the long-lead predictability of El Niño using a novel forecasting scheme based on a dynamic components model. *Climate Dynamics*, 48(3–4).
- Picaut, J., Masia, F. and Du Penhoat, Y. (1997) An advective-reflective conceptual model for the oscillatory nature of the ENSO. *Science*, 277(5326).
- Planton, Y., Vialard, J., Guilyardi, E., Lengaigne, M. and Izumo, T. (2018) Western Pacific Oceanic heat content: a better predictor of La Niña than of El Niño. *Geophysical Research Letters*, 45(18).
- Ramesh, N. and Murtugudde, R. (2013) All flavours of El Niño have similar early subsurface origins. *Nature Climate Change*, 3(1).
- Rasmusson, E.M. and Carpenter, T.H. (1982) Variations in tropical sea-surface temperature and surface wind fields associated with the Southern Oscillation/El Niño. *Monthly Weather Review*, 110(5).
- Rayner, N.A., Parker, D.E., Horton, E.B., Folland, C.K., Alexander, L.V., Rowell, D.P., Kent, E.C. and Kaplan, A. (2003) Global analyses of sea-surface temperature, sea ice, and night marine air temperature since the late nineteenth century. *Journal of Geophysical Research: Atmospheres*, 108(14).
- Ropelewski, C.F. and Halpert, M.S. (1987) Global and regional scale precipitation patterns associated with the El Niño/southern oscillation. *Monthly Weather Review*, 115(8).
- Ropelewski, C.F. and Halpert, M.S. (1989) Precipitation patterns associated with the high index phase of the Southern Oscillation. *Journal of Climate*, 2(3).
- Sparks, N. and Toumi, R. (2020) Pacific subsurface ocean temperature as a long-range predictor of South China tropical cyclone landfall. *Communications Earth & Environment*, 1(1).
- Srivastava, G., Chakraborty, A. and Nanjundiah, R.S. (2019) Multidecadal see-saw of the impact of ENSO on Indian and West African summer monsoon rainfall. *Climate Dynamics*, 52(11).
- Suarez, M.J. and Schopf, P.S. (1988) A delayed action oscillator for ENSO. *Journal of the Atmospheric Sciences*, 45(21).
- Sun, Q., Wu, B., Zhou, T.J. and Yan, Z.X. (2018) ENSO hindcast skill of the IAP-DecPreS near-term climate prediction system: comparison of full-field and anomaly initialization. *Atmospheric and Oceanic Science Letters*, 11(1).
- Takaya, Y., Kosaka, Y., Watanabe, M. and Maeda, S. (2021) Skillful predictions of the Asian summer monsoon one year ahead. *Nature Communications*, 12(1).
- Timmermann, A., An, S.I., Kug, J.S., Jin, F.F., Cai, W., Capotondi, A., Cobb, K., Lengaigne, M., McPhaden, M.J., Stuecker, M.F., Stein, K., Wittenberg, A.T., Yun, K.S., Bayr, T., Chen, H.C., Chikamoto, Y., Dewitte, B., Dommenges, D., Grothe, P., Guilyardi, E., Ham, Y.G., Hayashi, M., Ineson, S., Kang, D., Kim, S., Kim, W.M., Lee, J.Y., Li, T., Luo, J.J., McGregor, S., Planton, Y., Power, S., Rashid, H., Ren, H.L., Santoso, A., Takahashi, K., Todd, A., Wang, G., Wang, G., Xie, R., Yang, W.H., Yeh, S.W., Yoon, J., Zeller, E. and Zhang, X. (2018) El Niño–Southern Oscillation complexity. *Nature*, 559(7715).
- Vellinga, M. and Milton, S.F. (2018) Drivers of interannual variability of the East African “Long Rains”. *Quarterly Journal of the Royal Meteorological Society*, 144(712).
- Vigaud, N., Lyon, B. and Giannini, A. (2017) Sub-seasonal teleconnections between convection over the Indian Ocean, the East African long rains and tropical Pacific surface temperatures. *International Journal of Climatology*, 37(3).
- Wang, C. (2001) A unified oscillator model for the El Niño–Southern Oscillation. *Journal of Climate*, 14(1).
- Wang, C. (2018) A review of ENSO theories. *National Science Review*, 5(6).
- Wang, C., Weisberg, R.H. and Virmani, J.I. (1999) Western Pacific interannual variability associated with the El Niño–Southern Oscillation. *Journal of Geophysical Research: Oceans*, 104(C3).
- Weisberg, R.H. and Wang, C. (1997) A western Pacific oscillator paradigm for the El Niño–Southern Oscillation. *Geophysical Research Letters*, 24(7).
- Wooster, M.J., Perry, G.L. and Zoumas, A. (2012) Fire, drought and El Niño relationships on Borneo (Southeast Asia) in the pre-MODIS era (1980–2000). *Biogeosciences*, 9(1).

- Yang, S.C., Kalnay, E., Cai, M. and Rienecker, M.M. (2008) Bred vectors and tropical Pacific forecast errors in the NASA coupled general circulation model. *Monthly Weather Review*, 136(4).
- Yanto, Rajagopalan, B. and Zagona, E. (2016) Space–time variability of Indonesian rainfall at inter-annual and multi-decadal time scales. *Climate Dynamics*, 47(9–10), 2975–2989.
- Yuan, C., Tozuka, T., Landman, W.A. and Yamagata, T. (2014) Dynamical seasonal prediction of Southern African summer precipitation. *Climate Dynamics*, 42(11–12).
- Zhang, S., Wang, H., Jiang, H. and Ma, W. (2021) Evaluation of ENSO prediction skill changes since 2000 based on multimodel hindcasts. *Atmosphere*, 12(3).
- Zhao, S., Jin, F. and Stuecker, M.F. (2021) Understanding lead times of warm-water volumes to ENSO sea-surface temperature anomalies. *Geophysical Research Letters*, 48(19).

SUPPORTING INFORMATION

Additional supporting information may be found online in the Supporting Information section at the end of this article.

How to cite this article: Tsui, E.Y.L. & Toumi, R. (2022) Pacific subsurface temperature as a long-range indicator of El Niño, regional precipitation, and fire. *Quarterly Journal of the Royal Meteorological Society*, 1–16. Available from: <https://doi.org/10.1002/qj.4290>